

Bond-resolved silicene on Au(111) substrate

Ye Chen(陈烨), Wenya Zhai(翟文雅), Haoyuan Zang(臧浩原), Zengfu Ou(欧增福), Donghui Guo(郭东辉), and Jingcheng Li(李竟成)

Citatio: Chin. Phys. B, 2025, 34 (**9**): 096801. DOI: 10.1088/1674-1056/adee02
http://cpb.iphy.ac.cn; http://iopscience.iop.org/cpb

What follows is a list of articles you may be interested in

Emergent 3×3 charge order on the Cs reconstruction of kagome superconductor CsV_3Sb_5

Xianghe Han(韩相和), Zhongyi Cao(曹钟一), Zihao Huang(黄子豪), Zhen Zhao(赵振), Haitao Yang(杨海涛), Hui Chen(陈辉), and Hong-Jun Gao(高鸿钧)

Chin. Phys. B, 2025, 34 (**1**): 016801. DOI: 10.1088/1674-1056/ad8fa1

Visualizing interface states in In_2Se_3–WSe_2 monolayer lateral heterostructures

Da Huo(霍达), Yusong Bai(白玉松), Xiaoyu Lin(林笑宇), Jinghao Deng(邓京昊), Zemin Pan(潘泽敏), Chao Zhu(朱超), Chuansheng Liu(刘传胜), and Chendong Zhang(张晨栋)

Chin. Phys. B, 2023, 32 (**5**): 056803. DOI: 10.1088/1674-1056/acbaef

Enhanced photon emission by field emission resonances and local surface plasmon in tunneling junction

Jian-Mei Li(李健梅), Dong Hao(郝东), Li-Huan Sun(孙丽欢), Xiang-Qian Tang(唐向前), Yang An(安旸), Xin-Yan Shan(单欣岩), and Xing-Hua Lu(陆兴华)

Chin. Phys. B, 2022, 31 (**11**): 116801. DOI: 10.1088/1674-1056/ac8732

Two-dimensional Sb cluster superlattice on Si substrate fabricated by a two-step method

Runxiao Zhang(张润潇), Zi Liu(刘姿), Xin Hu(胡昕), Kun Xie(谢鹍), Xinyue Li(李新月), Yumin Xia(夏玉敏), and Shengyong Qin(秦胜勇)

Chin. Phys. B, 2022, 31 (**8**): 086801. DOI: 10.1088/1674-1056/ac70c1

Direct observation of the scaling relation between density of states and pairing gap in a dirty superconductor

Chang-Jiang Zhu(朱长江), Limin Liu(刘立民), Peng-Bo Song(宋鹏博), Han-Bin Deng(邓翰宾), Chang-Jiang Yi(伊长江), Ying-Kai Sun(孙英开), R Wu(武睿), Jia-Xin Yin(殷嘉鑫), Youguo Shi(石友国), Ziqiang Wang(汪自强), and Shuheng H. Pan(潘庶亨)

Chin. Phys. B, 2021, 30 (**10**): 106802. DOI: 10.1088/1674-1056/ac0903

RAPID COMMUNICATION

Bond-resolved silicene on Au(111) substrate

Ye Chen(陈烨)[1], Wenya Zhai(翟文雅)[1], Haoyuan Zang(臧浩原)[1], Zengfu Ou(欧增福)[2], Donghui Guo(郭东辉)[1,†], and Jingcheng Li(李竟成)[1,‡]

[1] *Guangdong Provincial Key Laboratory of Magnetoelectric Physics and Devices, School of Physics, Sun Yat-sen University, Guangzhou* 510275, *China*
[2] *College of Physics and Electronic Information Engineering, Guilin University of Technology, Guilin* 541004, *China*

(Received 2 May 2025; revised manuscript received 28 June 2025; accepted manuscript online 10 July 2025)

Silicene, a silicon analog of graphene, holds promise for next-generation electronics due to its tunable bandgap and larger spin–orbit coupling. Despite extensive efforts to synthesize and characterize silicene on metal substrates, bond-resolved imaging of its atomic structure has remained elusive. Here, we report the fabrication and bond-resolved characterization of silicene on Au(111) substrate. Three silicene phases tuned by surface reconstruction and annealing temperatures are achieved. Using CO-terminated scanning tunneling microscopy (STM) tips, we resolve these silicene phases with atomic precision, determining their bond lengths, local strain, and geometric configurations. Furthermore, we correlate these structural features with their electronic properties, revealing the effect of strain and substrate interactions on the electronic properties of silicene. This work establishes silicene's intrinsic bonding topology and resolves longstanding controversies in silicene research.

Keywords: scanning tunneling microscope, synthesis of silicene on Au(111), bond resolved imaging, bond length, local strain

PACS: 68.37.Ef, 82.75.Fq, 61.46.–w, 81.07.–b

DOI: 10.1088/1674-1056/adee02 **CSTR:** 32038.14.CPB.adee02

1. Introduction

The discovery of graphene has revolutionized materials science due to its remarkable electronic, mechanical, and thermal properties.[1] Silicene, the counterpart of graphene, shares most of graphene's exceptional properties owing to its analogous honeycomb structure.[2] In particular, silicene exhibits much stronger spin–orbit coupling than graphene, facilitating the emergence of the quantum spin Hall effect at experimentally accessible temperatures.[3] Moreover, its band gap can be tuned through external stimuli such as electric fields or chemical functionalization.[4–7] These enhanced properties make silicene a promising candidate for broad applications in fields like electronics, spintronics, chemical sensors, and beyond.[8–11] For instance, silicene-based field-effect transistors operating at room temperature have been demonstrated.[12]

Unlike graphene, silicene does not exist in nature, and synthetic approaches have to be developed.[13] The primary method for fabricating high-quality silicene involves epitaxial growth on metallic substrates.[14] Initial breakthroughs in synthesis were achieved using Ag(111)[15–20] and ZrB_2(0001)[19] surfaces, followed by exploration of various substrates including Ir(111), Au(111), MoS_2, among others.[22–35] Substrate selection critically impacts the structural and electronic properties of silicene, due to variations in lattice mismatch, interfacial bonding, and the buckled geometry of silicene. Epitaxial growth on different substrates produces different silicene superstructures.[14] Even on the same substrate, multiple superstructures can emerge depending on the coverage, substrate temperatures, and preparation methods, as seen with silicene on Ag(111)[8] and Au(111).[26,29,36] Determining the atomic arrangements of these superstructures is challenging due to the buckled geometry of silicene. Controversies and debates persist about superstructure models and their correlation with electronic properties.[8,14]

To address these issues, bond-resolved scanning tunneling microscope (BR-STM) images of the superstructures are essential, as they can provide detailed information such as bond length, bond angle, and local strain. These parameters are critical for determining the exact atomic structures of these superstructures, clarifying previous debates. Despite recent progress in the determination of atomic buckled geometry [37], achieving such high-resolution images with Si–Si bond resolution of these superstructures remains to be accomplished.

Here we present bond-resolved characterization of silicene synthesized on an Au(111) substrate. Three distinct superstructures are observed, whose formation can be controlled by adjusting annealing temperatures or surface reconstructions. Using CO-terminated tips, we acquire BR-STM images of all three phases. These images reveal that one su-

†Corresponding author. E-mail: guodonghui@mail.sysu.edu.cn
‡Corresponding author. E-mail: lijch73@mail.sysu.edu.cn

© 2025 Chinese Physical Society and IOP Publishing Ltd. All rights, including for text and data mining, AI training, and similar technologies, are reserved.

perstructure corresponds to a perfectly planar silicene lattice, with a measured Si–Si bond length of 2.46 Å. The other two superstructures are identified as strained silicene in buckled and non-buckled geometries, conclusively ruling out prior hypotheses of alloy formation. The strain in one superstructure reaches up to 20%, probably leading to a band gap of around 0.25 eV. Our results also indicate that the surface reconstruction plays an important role in the formation of silicene and its electronic properties.

2. Methods

The experiments were performed with a low-temperature ultra-high-vacuum (UHV) STM (Unisoku USM 1300). The Au(111) single crystal (MaTecK GmbH, 99.999%) was cleaned via repeated cycles of Ar^+ sputtering (1 eV) and subsequent annealing at 550 °C. Silicon was evaporated from a heated p-type Si wafer stripe (0.01 Ω·cm, 10 mm×2 mm ×0.5 mm) onto room-temperature Au(111) substrate. The coverage of silicon was controlled by evaporation time. The evaporation source temperature reached 1000 °C, monitored by an infrared pyrometer with 70% emissivity. The annealing of the Au(111) substrate with pre-evaporated silicon is described in the paper. A tungsten tip functionalized with a CO molecule was used for high-resolution imaging. The $\mathrm{d}I/\mathrm{d}V$ signals were recorded using a lock-in amplifier with a bias modulation of $V_{\mathrm{rms}} = 5$ mV. All the STM images were processed with WSxM.[38]

3. Results

Figure 1 summarizes the fabricated silicene on Au(111) substrate at different annealing temperatures. Silicon atoms are sublimed from a heated wafer (around 1000 °C) onto Au(111) surface kept at room temperature. At low coverage, silicon atoms form clusters on the surface, while the herringbone reconstruction of Au(111) is preserved (Fig. 1(a)). Increasing the coverage of silicon to a monolayer, no ordered structures appear (Fig. 1(b)). When the fully covered sample is annealed at 200 °C, nano-domains of ordered structures emerge, with sizes reaching about 4×4 nm^2. These ordered structures feature round protrusions arranged in a rectangular pattern (indicated by arrows in Fig. 1(c)). Further annealing at 250 °C results in large-area uniform phases with the same rectangular arrangements (named as RT-phase), probably formed by the merging of lower temperature nano-domains. A close-up view reveals two kinds of protrusion alternately arranged (highlighted with dashed ovals in Fig. 1(g)). This RT-phase was also observed with the silicon atoms evaporated on the hot Au(111) substrate kept at 260 °C,[24] and on Au(111) thin films on Si(111) substrate via surface segregation.[29] The exact structure of this phase, Si–Au alloy or pure silicene, is in debate.[26,29] It is also worth noting that similar protrusions are also observed on silicene prepared on Ag(111), except for their hexagon arrangement.[16,39–41]

Upon annealing at 300 °C, more complex periodic patterns emerge (Fig. 1(e)). A close-up view (Fig. 1(h)) reveals that these structures consist of small domains of hexagonal rings interconnected by disordered regions (named as HG-phase). This phase is similar to silicene $2\sqrt{3} \times 2\sqrt{3}$ reconstruction on Ag(111)[8] and has also been observed in Au(111) thin films on Si(111) through segregation.[29] In both systems, prior studies attribute the disordered areas to distortions in the hexagonal lattice.[16,29,42] The structural interpretations differ between substrates: for Ag(111), the silicene layer is proposed to adopt a buckled configuration,[16,42] whereas on Au(111), the silicene remains planar.[29]

Elevated annealing at 350 °C induces another drastic structural transformation. The system reverts to a configuration dominated by protrusions, though now organized into an elongated zigzag arrangement (named as ZZ-phase), as highlighted by dashed lines in Fig. 1(f). At the same time, pore-like features emerge within the lattice (highlighted by dashed oval in Fig. 1(f)). Close-up views reveal that these pores consist of a few hexagonal rings. This phase is also observed in previous reports, yet not analyzed in detail.[34]

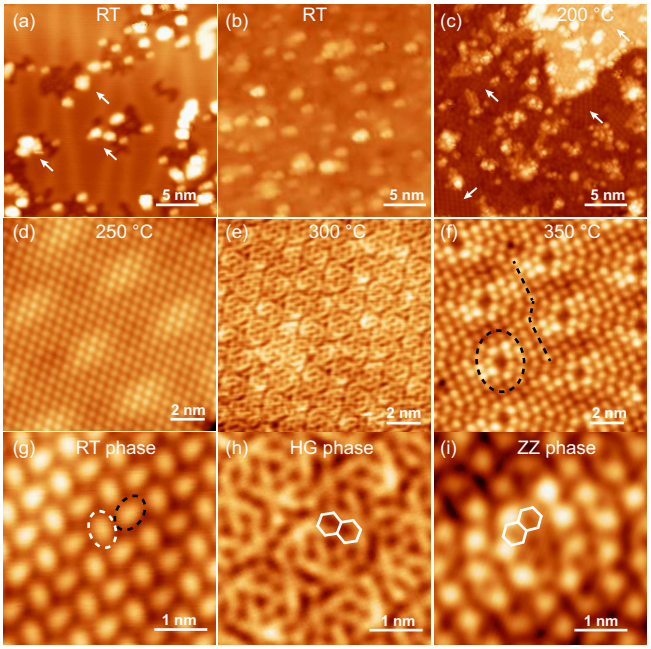


Fig. 1. Synthesis of silicene on Au(111) substrate. (a) STM image of Au(111) substrate after low-coverage deposition of silicon atoms. Arrows indicate the formed silicon clusters. (b) STM image of Au(111) substrate fully covered with evaporated silicon atoms. (c)–(f) STM images of the same sample after annealing at 200 °C (c), 250 °C (d), 300 °C (e), and 350 °C (f), respectively, as noted on the images. Arrows in (c) indicate the ordered structures. Dashed line (oval) in (f) indicates the elongated zigzag arrangement (pore-like features). (g)–(i) Close-up view of the images in (d)–(f), respectively. Dashed ovals in (g) highlight the two kinds of protrusions. Hexagons in (h) and (i) highlight the formed hexagonal rings. Tunneling parameters: $V = 1$ V for images (a)–(f); $V = -0.1$ V for image (g); $V = -4$ mV for image (h); and $V = 0.3$ V for image (i).

In addition to temperature, the structural evolution of silicene on Au(111) is strongly influenced by substrate reconstruction. The herringbone reconstruction of Au(111) can be modified through silicon deposition and subsequent annealing. After low-coverage silicon deposition followed by 200 °C annealing, the surface transitions from its characteristic herringbone pattern to networks formed by triangular domain walls (named as triangular reconstruction, Fig. 2(a)), with an average area of 5×5 nm^2. High-resolution imaging (inset, Fig. 2(a)) demonstrates that Au atoms retain a close-packed arrangement, though with different surface ripple (supplementary Fig. S3). Notably, the interatomic distance between neighboring Au atoms decreases from 2.72 Å in the herringbone reconstruction to approximately 2.6 Å in the triangular reconstructions (supplementary Fig. S3).

On the triangular reconstructed surface, silicon atoms form protrusions resembling those in Figs. 1(c), 1(d), and 1(f) at low coverages (Fig. 2(b)). These protrusions are not organized into ordered phases. Increasing the silicon coverage promotes phase ordering, as shown in Fig. 2(c), where coexisting rectangular patterns, elongated zigzag motifs, and pore-like features emerge. Beyond monolayer coverage, the zigzag motif dominates (Fig. 2(d)), with second- and third-layer silicene adopting similar configurations. Annealing further enhances structural uniformity: both half- and full-coverage samples exhibit more ordered zigzag patterns after annealing at 300 °C (Figs. 2(e) and 2(f)), analogous to the configuration observed after 350 °C annealing in Fig. 1(f). It is worth noting that unlike silicene prepared on herringbone-reconstructed surfaces, annealing does not alter the superstructure phase in this system.

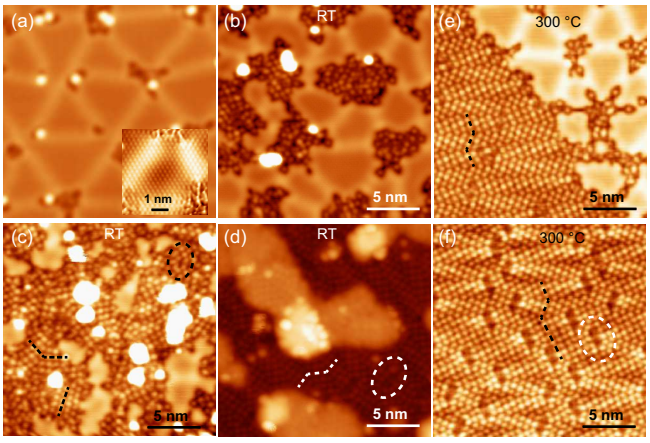


Fig. 2. Effect of surface reconstruction on the synthesis of silicene. (a) STM image of reconstructed Au(111) surface induced by low-coverage silicon deposition followed by annealing. Inset shows a close-up view with atomic resolution. (b)–(d) STM images of the same surface after additional silicon deposition at room temperature, with coverages of approximately 0.2 monolayers (b), 0.6 monolayers (c), and 1.5 monolayers (d). (e) STM image of a half-coverage silicon surface prepared as in (b) after annealing at 300 °C. (f) STM image of full-coverage surface prepared as in (b) after annealing at 300 °C. Dashed lines and ovals indicate the rectangular patterns, the elongated zigzag pattern, and pore-like features. Tunneling parameters: $V = 1$ V for all the images.

To resolve the structural details of the three observed phases, BR-STM imaging was performed using a CO-terminated tip. Figure 3 compares the STM images acquired with metal tip and CO-terminated tip for the three phases. For the RT-phase, instead of rectangular protrusion patterns, the BR-STM image reveals well-defined hexagonal structures (Figs. 3(a) and 3(b)). These hexagon structures are thus identified as the silicene honeycomb lattices, which resolves prior debates about its formation on Au(111).[26,29] The two protrusion types are identified, as one protrusion is brighter at the center of the silicene ring, while the other type of protrusion is brighter over the Si–Si bond, likely due to the mismatch between silicene lattices and underlying Au substrate. The BR-STM images also indicate the buckled geometry of silicene, as some silicon sites appear dark on the image (highlighted by red circles in Fig. 3(b)). The buckled height is determined to be around 0.24 Å (supplementary Fig. S4), lower than the value of silicene grown on other substrates.[14] Additionally, the BR-STM images reveal anisotropic strain in silicene (highlighted by the imposed model structure in Fig. 3(b)), reaching magnitudes of 20%. This finding aligns with prior low energy electron diffraction (LEED) studies reporting significant strain in silicene.[43]

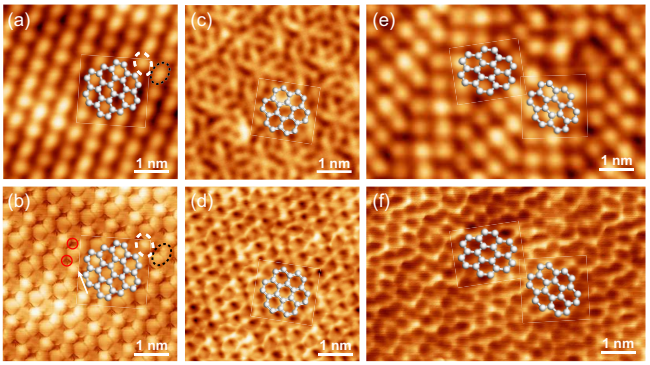


Fig. 3. Bond-resolved STM images of silicene. (a), (c), (e) STM images of the three primary phases recorded with a metal tip. (b), (d), (f) are the corresponding STM images recorded with a CO-terminated tip. Chemical model structures are superimposed on the images for clarity. Tunneling parameters: (a) $V = 400$ mV, (b) $V = -4$ mV, (c) $V = 100$ mV, (d) $V = 2$ mV, (e) $V = -2$ mV, (f) $V = 2$ mV. (a)–(e) are constant-current images, while (f) is a constant-height image.

In the case of HG-phase, while metal-tip imaging depicts ordered hexagonal rings interconnected by disordered regions, BR-STM image displays a defect-free, uniform honeycomb lattice (Figs. 3(c) and 3(d)). As shown in the supplementary Fig. S6, the images with metal tip at different bias values show different features, indicating their origin from the convolution of topographic and electronic features. STM image with CO-terminated tip at small tip-sample distances ($V = 2$ mV, $I = 1$ nA) successfully resolves the Si–Si bond. The silicene layer in this phase is fully planar, exhibiting no measurable strain. The Si–Si bond length is determined to be 2.46 ± 0.07 Å (lattice constant: 4.27 Å), agreeing well with

the simulation of planar silicene.[28] For the ZZ-phase, showing protrusions patterns like the RT-phase, BR-STM imaging also displays hexagonal structures (Figs. 3(c)–3(f)). Unlike the RT-phase, the ZZ-phase adopts a planar geometry with slight ripple features and non-uniform strain, as highlighted by superimposed structural models (Fig. 3(f)).

To probe the electronic characteristics of the three silicene phases, differential conductance ($\mathrm{d}I/\mathrm{d}V$) spectra were recorded (Fig. 4). The $\mathrm{d}I/\mathrm{d}V$ spectrum taken on the RT-phase and HG-phase exhibit a general V-shaped feature around the Fermi level. The spectrum of RT-phase shows a flat bottom, indicating a band gap opening of approximately 0.25 eV (Fig. 4(a)). We speculate that the small gap opening is due to the uniaxial strain in silicene, consistent with simulations predicting that uniaxial strain induces uniform gap opening in silicene's electronic structure.[44] This result aligns with high-resolution angle-resolved photoemission spectroscopy (HRARPES) measurements,[26] which reported a similar band gap opening. Previous ARPES measurements also show that the Dirac cones of RT-phase and HG-phase are shifted to around -0.5 eV and -0.7 eV below the Fermi level.[24,32] Kink-like features at these energy locations do appear on the spectra of RT-phase and HG-phase, which could reflect the signatures of Dirac cones. In contrast, the spectra taken on ZZ-phase display a pronounced, position-independent dip (Figs. 4 and S8), suggesting Dirac cone behavior at the Fermi level. Its relation to Dirac cone behavior may require further experimental verification. The conductance maps of the three phases, which demonstrate the spatial distribution of local density of states (LDOS), are also recorded (supplementary Figs. S5 and S6). These $\mathrm{d}I/\mathrm{d}V$ maps show strong modulations of LDOS by the substrate, indicating a strong coupling between the silicene layer and the underlying Au(111) substrate.

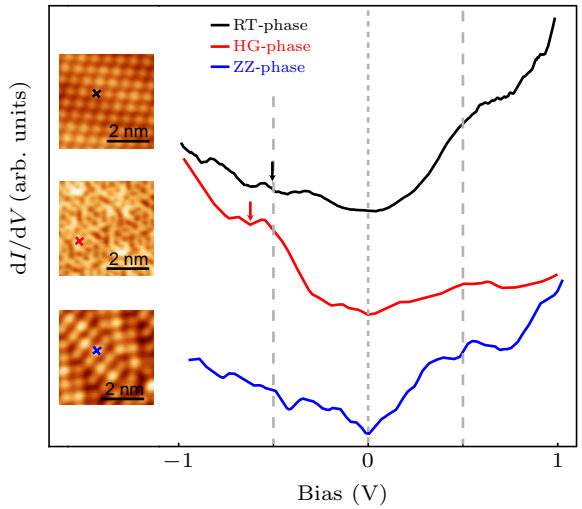


Fig. 4. Electronic properties of silicene on Au(111) substrate. $\mathrm{d}I/\mathrm{d}V$ spectra recorded for the three silicene phases (RT-phase: black curve; HG-phase: red curve; ZZ-phase: blue curve), with the locations of the spectra indicated in the inset images. The spectra are shifted vertically for clarity. Arrows indicate the kink features.

4. Discussion

The silicene-Au(111) interface constitutes a highly complex system. While bond-resolved STM (BR-STM) imaging has successfully resolved silicene's atomic structure, the precise interface configurations and underlying substrate details remain unresolved. The observed phase transitions in silicene with annealing temperature likely arise from a change of surface reconstruction. For instance, the transition from the RT-phase to the ZZ-phase is correlated with a shift from the herringbone reconstruction to a triangular reconstruction. The specific Au reconstruction in the HG phase remains unclear, though we hypothesize it involves a distinct reconstruction pattern. As the substrate surface evolves (e.g., rippling, changes in interatomic distances), the lattice mismatch between silicene and Au(111) varies, potentially inducing differences in silicene's bonding, buckling, and strain, thus resulting in the different phases observed in the experiments. Additionally, charge transfer between silicene and the substrate is configuration-dependent. These substrate-mediated strains, chemical bonding, and charge transfer collectively modulate the electronic properties of silicene.

5. Conclusion

In conclusion, we have demonstrated the controlled synthesis of silicene on Au(111). The annealing temperatures play a major role in the formation of different silicene phases, while the underlying mechanism is the gold surface reconstruction induced by annealing. The coverage also has an effect but only matters for the case of silicon deposited on a surface with triangular reconstruction. Even in this case, annealing can promote structural uniformity, mainly due to the enhanced diffusion of silicon on the surface. The bond-resolved STM imaging directly reveals the atomic-scale structure of three silicene phases, enabling precise determination of bond lengths, strain, and local geometry. These results unambiguously resolve debates on silicene structural properties on Au(111), while also shedding light on silicene configurations formed on analogous substrates such as Ag(111). These results advance the field by clarifying inconsistencies in prior studies and paving the way for tailored silicene-based materials in future electronic or quantum devices.

Acknowledgments

Project supported by the National Natural Science Foundation of China (Grant No. 12474181), the Guangdong Basic and Applied Basic Research Foundation (Grant Nos. 2021B0301030002 and 2024A1515010656), and the Guangdong Science and Technology Project (Grant No. 2021QN02X859). The experiments reported

were conducted at the Guangdong Provincial Key Laboratory of Magnetoelectric Physics and Devices (Grant No. 2022B1212010008).

References

[1] Novoselov K S, Fal'ko V I, Colombo L, Gellert P R, Schwab M G and Kim K 2012 *Nature* **490** 192

[2] Jose D and Datta A 2014 *Chem. Res.* **47** 593

[3] Liu C C, Feng W and Yao Y 2011 *Phys. Rev. Lett.* **107** 076802

[4] Ni Z, Liu Q, Tang K, Zheng J, Zhou J, Qin R, Gao Z, Yu D and Lu J 2012 *Nano Lett.* **12** 113

[5] Quhe R, Fei R, Liu Q, Zheng J, Li H, Xu C, Ni Z, Wang Y, Yu D, Gao Z and Lu J 2012 *Sci. Rep.* **2** 853

[6] Du Y, Zhuang J, Liu H, Xu X, Eilers S, Wu K, Cheng P, Zhao J, Pi X, See K W, Peleckis G, Wang X and Dou S X 2014 *ACS Nano* **8** 10019

[7] Qiu J, Fu H, Xu Y, Oreshkin A I, Shao T, Li H, Meng S, Chen L and Wu K 2015 *Phys. Rev. Lett.* **114** 126101

[8] Zhao J, Liu H, Yu Z, Quhe R, Zhou S, Wang Y, Liu C C, Zhong H, Han N, Lu J, Yao Y and Wu K 2016 *Prog. Mater. Sci.* **83** 24

[9] Shan G, Tan H, Ma R, Zhao H and Huang W 2023 *Nanoscale* **15** 2982

[10] Liu M, Cheng Z, Zhang X, Li Y, Jin L, Liu C, Dai X, Liu Y, Wang X and Liu G 2023 *Chin. Phys. B* **32** 096303

[11] Xie H, Lü X L and Yang J E 2023 *Chin. Phys. B* **33** 018502

[12] Tao L, Cinquanta E, Chiappe D, Grazianetti C, Fanciulli M, Dubey M, Molle A and Akinwande D 2015 *Nat. Nanotechnol.* **10** 227

[13] Man Q, An Y, Shen H, Wei C, Xiong S and Feng J 2023 *Mater. Today* **67** 566

[14] Masson L and Prévot G 2023 *Nanoscale Adv.* **5** 1574

[15] Vogt P, De Padova P, Quaresima C, Avila J, Frantzeskakis E, Asensio M C, Resta A, Ealet B and Le Lay G 2012 *Phys. Rev. Lett.* **108** 155501

[16] Feng B, Ding Z, Meng S, Yao Y, He X, Cheng P, Chen L and Wu K 2012 *Nano Lett.* **12** 3507

[17] Lin C L, Arafune R, Kawahara K, Tsukahara N, Minamitani E, Kim Y, Takagi N and Kawai M 2012 *Appl. Phys. Express* **5** 045802

[18] Jamgotchian H, Colignon Y, Hamzaoui N, Ealet B, Hoarau J Y, Aufray B and Bibérian J P 2012 *J. Phys.: Condens. Matter* **24** 172001

[19] Chen L, Liu C C, Feng B, He X, Cheng P, Ding Z, Meng S, Yao Y and Wu K 2012 *Phys. Rev. Lett.* **109** 056804

[20] Enriquez H, Vizzini S, Kara A, Lalmi B and Oughaddou H 2012 *J. Phys.: Condens. Matter* **24** 314211

[21] Fleurence A, Friedlein R, Ozaki T, Kawai H, Wang Y and Yamada-Takamura Y 2012 *Phys. Rev. Lett.* **108** 245501

[22] Meng L, Wang Y, Zhang L, Du S, Wu R, Li L, Zhang Y, Li G, Zhou H, Hofer W A and Gao H J 2013 *Nano Lett.* **13** 685

[23] Aizawa T, Suehara S and Otani S 2014 *J. Phys. Chem. C* **118** 23049

[24] De Crescenzi M, Berbezier I, Scarselli M, Castrucci P, Abbarchi M, Ronda A, Jardali F, Park J and Vach H 2016 *ACS Nano* **10** 11163

[25] Huang L, Zhang Y F, Zhang Y Y, Xu W, Que Y, Li E, Pan J B, Wang Y L, Liu Y, Du S X, Pantelides S T and Gao H J 2017 *Nano Lett.* **17** 1161

[26] Sadeddine S, Enriquez H, Bendounan A, Kumar Das P, Vobornik I, Kara A, Mayne A J, Sirotti F, Dujardin G and Oughaddou H 2017 *Sci. Rep.* **7** 44400

[27] Li G, Zhang L, Xu W, Pan J, Song S, Zhang Y, Zhou H, Wang Y, Bao L, Zhang Y, Du S, Ouyang M, Pantelides S T and Gao H 2018 *Adv. Mater.* **30** 1804650

[28] Stepniak-Dybala A, Dyniec P, Kopciuszyski M, Zdyb R, Jałochowski M and Krawiec M 2019 *Adv. Funct. Mater.* **29** 1906053

[29] Stępniak-Dybala A and Krawiec M 2019 *J. Phys. Chem. C* **123** 17019

[30] Nicholls D, Fatima, Çakır D and Oncel N 2019 *J. Phys. Chem. C* **123** 7225

[31] Wiggers F B, Fleurence A, Aoyagi K, Yonezawa T, Yamada-Takamura Y, Feng H, Zhuang J, Du Y, Kovalgin A Y and De Jong M P 2019 *2D Mater.* **6** 035001

[32] Sato Y, Fukaya Y, Cameau M, Kundu A K, Shiga D, Yukawa R, Horiba K, Chen C H, Huang A, Jeng H T, Ozaki T, Kumigashira H, Niibe M and Matsuda I 2020 *Phys. Rev. Mater.* **4** 064005

[33] Leoni T, Hogan C, Zhang K, Daher Mansour M, Bernard R, Parret R, Resta A, Colonna S, Borensztein Y, Ronci F, Prévot G and Masson L 2021 *J. Phys. Chem. C* **125** 17906

[34] Kopciuszyński M, Stępniak-Dybala A, Zdyb R and Krawiec M 2024 *Nano Lett.* **24** 2175

[35] Stępniak-Dybala A and Krawiec M 2025 *Surf. Interfaces* **59** 105937

[36] Deniz O, Sánchez-Sánchez C, Dumslaff T, Feng X, Narita A, Müllen K, Kharche N, Meunier V, Fasel R and Ruffieux P 2017 *Nano Lett.* **17** 2197

[37] Pawlak R, Drechsel C, D'Astolfo P, Kisiel M, Meyer E and Cerda J I 2020 *Proc. Natl. Acad. Sci. USA* **117** 228

[38] Horcas I, Fernández R, Gómez-Rodríguez J M, Colchero J, Gómez-Herrero J and Baro A M 2007 *Rev. Sci. Instrum.* **78** 013705

[39] Chiappe D, Grazianetti C, Tallarida G, Fanciulli M and Molle A 2012 *Adv. Mater.* **24** 5088

[40] Arafune R, Lin C L, Kawahara K, Tsukahara N, Minamitani E, Kim Y, Takagi N and Kawai M 2013 *Surf. Sci.* **608** 297

[41] Liu Z L, Wang M X, Xu J P, Ge J F, Lay G L, Vogt P, Qian D, Gao C L, Liu C and Jia J F 2014 *New J. Phys.* **16** 075006

[42] Jamgotchian H, Ealet B, Colignon Y, Maradj H, Hoarau J Y, Biberian J P and Aufray B 2015 *J. Phys.: Condens. Matter* **27** 395002

[43] Nazzari D, Genser J, Ritter V, Bethge O, Bertagnolli E, Ramer G, Lendl B, Watanabe K, Taniguchi T, Rurali R, Kolíbal M and Lugstein A 2021 *J. Phys. Chem. C* **125** 9973

[44] Zhao H 2012 *Phys. Lett. A* **376** 3546